



Science Arts & Métiers (SAM)

is an open access repository that collects the work of Arts et Métiers Institute of Technology researchers and makes it freely available over the web where possible.

This is an author-deposited version published in: <https://sam.ensam.eu>
Handle ID: <http://hdl.handle.net/10985/24967>

To cite this version :

Clément DESPRES, Christine BIATEAU, Michel CASTAINGS, Nicolas QUAEGEBEUR, Patrice MASSON, Eric DUCASSE - Characterization of viscoelastic moduli and thickness of isotropic, viscoelastic plates using multi-modal Lamb waves - NDT& E International - Vol. 144, p.103095 - 2024

Any correspondence concerning this service should be sent to the repository

Administrator : scienceouverte@ensam.eu



Characterization of viscoelastic moduli and thickness of isotropic, viscoelastic plates using multi-modal Lamb waves

Clément Despres^{a,b,c,*}, Christine Biateau^{a,b}, Michel Castaings^{a,b}, Nicolas Quaegebeur^c, Patrice Masson^c, Eric Ducasse^{a,b}

^a Univ. Bordeaux, CNRS, Bordeaux INP, I2M, UMR 5295, F-33400, Talence, France

^b Arts et Métiers Institute of Technology, CNRS, Bordeaux INP, Hesam Université, I2M, UMR 5295, F-33400, Talence, France

^c Dept Mechanical Engineering, GAUS/CRASH-UdeS, Univ. Sherbrooke, Sherbrooke, J1K 2R1, Québec, Canada

ABSTRACT

Keywords:

Lamb waves

Sensitivity functions

Characterization of viscoelastic moduli

Characterization of thickness

Air-coupled transducers

This paper presents an approach exploiting the sensitivity of Lamb waves for characterizing the viscoelastic moduli and thickness of plates. The analytical sensitivity functions are first derived in the case of an isotropic plate and are integrated into an iterative inverse problem to optimize its viscoelastic moduli and thickness based on a zero-finding approach (Gauss–Newton algorithm for a multivariable problem). This method is validated numerically for a viscoelastic plate and shows high accuracy and low computational cost when compared to existing methods. Experimental validation demonstrates the ability of the algorithm to assess simultaneously the viscoelastic moduli and the thickness of isotropic plate-like structures.

1. Introduction

The characterization of the elastic properties of materials is critical for their use in a wide range of applications. Ultrasonic inspection techniques have been used over the years for non-destructive evaluation (NDE) of the viscoelastic moduli of materials. Some of the ultrasonic techniques require direct contact [1] with the tested sample, or immersion in water [2] to ensure a good transfer of energy between the transducer and the sample. The immersion technique usually requires access to both faces of the material but can also be used in a unilateral access configuration [3] which is more convenient in an industrial context. However, the tested sample should fit into the immersion tank, which can be a challenge for large structures.

The propagation of ultrasonic guided waves is strongly dependent upon material properties such as thickness, density and elasticity moduli, making them useful for characterization. Lamb waves can be generated and measured with a non-contact setup in air by using laser [4]. However, the cost and the required accuracy for laser set-up constitute serious drawbacks for in-situ applications. Ultrasonic capacitive air-coupled transducers allow generating and detecting ultrasound in air with a fairly large frequency bandwidth [5]. This technology is more convenient than laser because of its cost and portability, and is easily compatible with the industrial environment.

It has been shown that by the measuring of the phase velocity of several guided wave modes, the elastic moduli of the material can

be inferred [6,7] as well as the thickness of the tested sample [8,9]. However, to the best of our knowledge, none of the existing methods can evaluate viscoelastic moduli and the thickness simultaneously.

A natural approach for assessing material properties is to solve an inverse problem consisting in minimizing the difference between numerical and experimental data (e.g., time domain signals, group or phase velocity). A number of minimization algorithms have been developed to solve this type of inverse problem: Simplex algorithm [10], Gauss–Newton algorithms [11,12], evolutionary algorithms [13,14], animal flocking behavior algorithms [15,16] or more recently the training of a neural network [17]. The choice of the algorithm depends on several factors such as the conditioning of the inverse problem, the type of the measured data, etc. With most of these algorithms, the number of iterations required to converge can be huge depending on the initial guess and the listed factors (for example about hundred iterations for Simplex [10] and PSO [16]) in contrast to a Gauss–Newton scheme that converges rapidly (about ten iterations [11]), provided that the required assumptions are met. The main drawback of the Gauss–Newton method is that the calculation of the Jacobian matrix can be a heavy calculation since it is usually necessary to approximate the terms inside the matrix because there is generally no analytical expression.

In this paper, the viscoelastic moduli and the thickness of an isotropic plate are estimated, simultaneously, using a Gauss–Newton

* Corresponding author at: Dept Mechanical Engineering, GAUS/CRASH-UdeS, Univ. Sherbrooke, Sherbrooke, J1K 2R1, Québec, Canada.

E-mail address: Clement.Despres@USherbrooke.ca (C. Despres).

algorithm. In addition, the terms inside the Jacobian matrix, which represents the sensitivity of Lamb modes to viscoelastic moduli and thickness, are expressed analytically to allow a fast and accurate estimation of the sought parameters. Section 2 is dedicated to the calculation of the sensitivity function. Section 3 presents the development of the mathematical formalism of the Gauss-Newton procedure using analytical form of the sensitivity function. Section 4 presents the experimental characterization of a reference viscoelastic isotropic plate using the abovementioned formalism.

2. Sensitivity of lamb waves to viscoelastic moduli, thickness and density

A sensitivity study is the first step in the process of assessing the viscoelastic moduli and thickness from measured or simulated data. It has been shown that some Lamb wave modes are sensitive to specific elastic moduli, thickness and density while others are insensitive to these parameters in a given frequency bandwidth [18]. Within the context of solving an inverse problem to estimate the viscoelastic moduli and thickness from Lamb waves, it is advisable to use sensitive modes. The sensitivity of a Lamb wave mode to a given parameter p_j among a set of parameters \mathbf{p} is usually defined as the variation in wavenumber $k(\omega)$ produced by a perturbation δp_j of this parameter [19]. This definition can be viewed as the derivative of the wavenumber with respect to the parameter p_j as presented in Eq. (1) :

$$S_{p_j}(\omega) = \frac{\partial k(\mathbf{p}, \omega)}{\partial p_j} \quad (1)$$

where $\omega = 2\pi f$ denotes the angular frequency. The wavenumber $k(\mathbf{p}, \omega)$ is determined from the dispersion equation whose complexity depends on the characteristics of the medium of propagation e.g, the material anisotropy and the stacking sequence in the case of composite material. For isotropic plates, the Lamb modes satisfy the transcendental equation given by Eq. (2) [20] :

$$\frac{\omega^4}{4k^2 q^2 c_T^4} = 1 - \frac{b \tan(bh + \alpha)}{q \tan(qh + \alpha)} \quad (2)$$

where h is the half thickness of the plate ($h = e/2$), $\alpha = \pi/2$ if the mode is antisymmetric and $\alpha = 0$ if the mode is symmetric, $b = \sqrt{k_L^2 - k^2}$, $k_L = \omega/c_L$ where $c_L = \sqrt{C_{11}/\rho}$, $q = \sqrt{k_T^2 - k^2}$, $k_T = \omega/c_T$ where $c_T = \sqrt{C_{66}/\rho}$. The elastic moduli C_{11} and C_{66} correspond to the elastic moduli C_{1111} and C_{1212} respectively using Voigt notation, with 1 the axis normal to the plate and 2 the Lamb wave propagation direction. Usually this equation is solved numerically to find the complex (k, ω) solution pairs. Since the function $k(\mathbf{p}, \omega)$ cannot be solved analytically, the expression of its derivative is complex. Thus, Eq. (1) can be approximated by finite differences :

$$S_{p_j}^{(i)}(\omega) \approx \sum_{i=i_{\min}}^{i_{\max}} \frac{N_i k(p + i\delta p_j)}{D \delta p_j} + O(\delta p_j^{(i)}) \quad (3)$$

where i denotes the order of approximation of the first order derivative; N_i and D are constants dependent on the order i . The values of these parameters are given in Table 1.

Because the material is isotropic, one can calculate analytically the sensitivity function $S_{p_j}(\omega)$ for a given mode. Let us consider the calculation of the sensitivity function of Lamb waves to a given parameter p_j : $\partial k / \partial p_j$. Applying the derivative with respect to p_j to both sides of the Eq. (2) and simplifying the expression leads to:

$$\frac{\partial k}{\partial p_j} = \frac{\beta_L \frac{\partial k_L^2}{\partial p_j} + \beta_T \frac{\partial k_T^2}{\partial p_j} + \beta_h \frac{\partial h}{\partial p_j}}{2k(\beta_L + \beta_T) + T_q^2(2k\mu + \nu)} \quad (4)$$

with:

Table 1

Coefficient values for the first derivative approximation at orders 1, 2 and 4.

i	i_{\min}	i_{\max}	D	N_{-2}	N_{-1}	N_0	N_1	N_2
1	0	1	1			-1	1	
2	-1	1	2		-1	0	1	
4	-2	2	12	1	-8	0	8	-1

Table 2

Coefficient values for the derivative of k_L^2 , k_T^2 and h with respect to the parameters C_{11} , C_{66} , h and ρ .

	∂k_L^2	∂k_T^2	∂h
∂C_{11}	$-\omega^2 \rho / C_{11}$	0	0
∂C_{66}	0	$-\omega^2 \rho / C_{66}$	0
∂h	0	0	1
$\partial \rho$	ω^2 / C_{11}	ω^2 / C_{66}	0

$$\begin{cases} \beta_L = -(\gamma_0 T_q) & \beta_T = (T_0 \gamma_q - \mu T_q^2) & \beta_h = -(\eta_0 T_q - \eta_q T_k) \\ \gamma_{0,q} = \frac{1}{2} \left(\frac{T_{0,q}^2}{b^2, q^2} (1 + T_{0,q} h) + h \right) & \eta_{0,q} = b^2, q^2 + T_{0,q}^2 \\ T_q = q \tan(qh + \alpha) & T_k = b \tan(bh + \alpha) \\ \mu = \frac{-k_T^2}{4k^2 q^4} (k_T^2 - 2q^2) & \nu = \frac{-k_T^4}{2k^3 q^4} (q^2 - k^2) \end{cases}$$

and the value of the derivatives $\partial k_L^2 / \partial p_j$, $\partial k_T^2 / \partial p_j$ and $\partial h / \partial p_j$ for parameters $p_j = C_{11}$, C_{66} , h and ρ are given in Table 2.

The sensitivity functions are calculated for the case of an isotropic Perspex plate using viscoelastic moduli provided in Ref. [21], the values of which are: $C_{11} = (8.5 + 0.36i) \pm (0.1 + 0.02i)$ GPa and $C_{66} = (2.5 + 0.1i) \pm (0.2 + 0.1i)$ GPa with a thickness $e = 3.90$ mm measured using a caliper. In that paper, a Hysteretic model is used to model the viscoelasticity of the material. This model assumes that the imaginary parts of the viscoelastic moduli are not frequency-dependent [22]. To made reliable comparison and because the plate as well as the frequency magnitude are almost the same, a Hysteretic model is used in the following development.

The sensitivity to each parameters $p_j \in \mathbf{p}$, with $\mathbf{p} = [e, \rho, C'_{11}, C'_{66}, C''_{11}, C''_{66}]$ is calculated according to Eq. (1) for each mode propagating in the frequency band 100–500 kHz. The sensitivity is then multiplied by $\delta p_j / k(\mathbf{p}, \omega)$ ($\delta p_j = 0.05 \times p_j$) to quantify the effect of 5% change in each parameter p_j on wavenumbers, as presented in [14].

The sensitivity of Lamb modes to parameters in \mathbf{p} is represented in Fig. 1(a–f) for a Perspex plate. The sensitivity is encoded by color gradient overlaid on the dispersion curves of Lamb modes. This representation allows modes to be identified (by their dispersion curve) as well as the frequency zones for high sensitivity to material parameters \mathbf{p} . Blue areas represent part of the dispersion curves that undergo a decrease in their wavenumber and red areas represent an increase in their wavenumber. The black zones represent areas where $|S_{p_j}(\omega) \times \delta p_j / k(\mathbf{p}, \omega)| > 10\%$ and are considered as zones of high sensitivity. Fig. 1(a–d) presents changes in the real part of the wavenumber, k' , caused by a change in material properties $e, \rho, C'_{11}, C'_{66}$, respectively while Fig. 1(e–f) presents changes in attenuation (imaginary part of the wavenumber, k'') caused by a change in C''_{11}, C''_{66} , respectively. This choice was done because k' and k'' are used later on to assess the real and imaginary parts of the sought viscoelastic moduli, respectively.

The Fig. 1(a–b) shows that all modes are sensitive to the thickness and to the density of the plate. High-order modes are particularly sensitive to these properties in the vicinity of their cut-off frequencies as shown by the black zones. A small change in density or thickness is shown to significantly shift these cut-off frequencies and to cause large changes in wavenumbers around the cut-off frequencies. Fig. 1(c–d) shows the sensitivity of the Lamb modes to C'_{11} and C'_{66} , respectively.

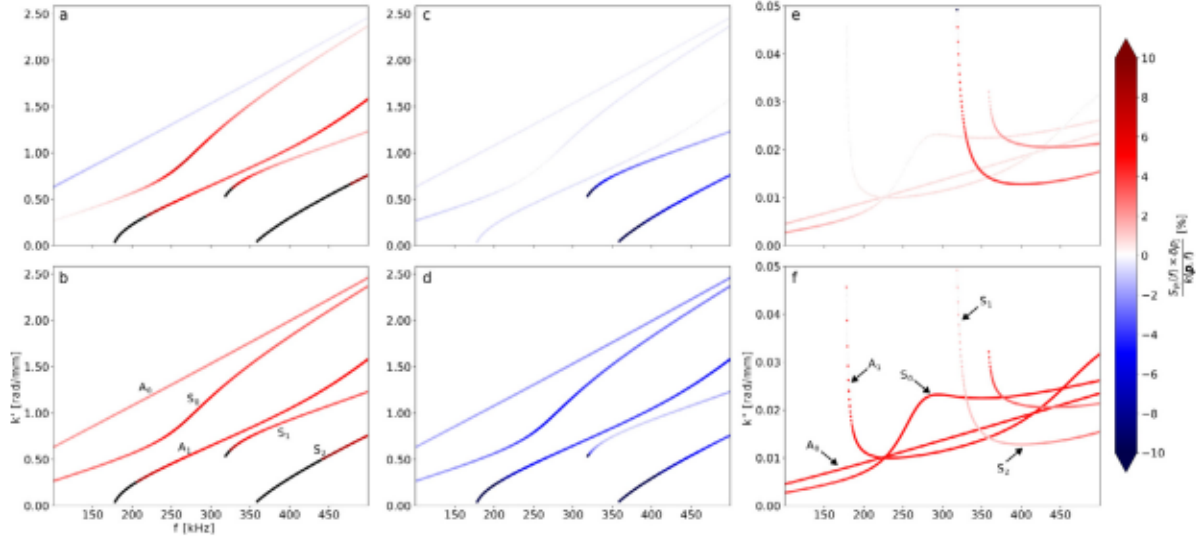


Fig. 1. Sensitivity function $S_{p_j}(\omega) \times \delta p_j / k(\mathbf{p}, \omega)$ as a function of frequency for Perspex plate of thickness 3.9 mm. (a): e , (b): ρ , (c): C'_{11} , (d): C''_{66} , (e): C''_{11} , (f): C''_{66} .

It is important to note that mainly S_1 and S_2 modes are sensitive to C'_{11} which makes them essential to quantify C'_{11} . Moreover, this sensitivity is highest close to their cut-off frequency. All modes in the investigated frequency range are sensitive to C''_{66} but A_1 and S_2 are the most sensitive to this parameter and this is particularly true in the vicinity of their cut-off frequency. Finally, Fig. 1(e-f) presents the changes in attenuation caused by a 5% change in C''_{11} and C''_{66} , respectively. Some of the trends observed for the sensitivity of k' to C'_{11} and C'_{66} are observable for the sensitivity of k'' to C''_{11} and C''_{66} . Modes S_1 and S_2 are still the most sensitive to C''_{11} while all modes are equally sensitive to C''_{66} .

3. Inverse problem formulation for the characterization of viscoelastic moduli and thickness

Usually, to find the material properties \mathbf{p} of a plate from the wavenumber of propagating Lamb wave, an inverse problem is solved using an optimization algorithm that minimizes a cost function $D(\mathbf{p})$. The cost function can be defined as the distance between a target wavenumber $k_m^{tar}(\omega)$ and a forward wavenumber $k_m(\mathbf{p}, \omega)$, calculated by solving the dispersion equation with known \mathbf{p} :

$$D(\mathbf{p}) = \sum_m \left(\sum_i^{N_\omega} \left(k_{m,i}^{tar}(\omega_i) - k_{m,i}(\mathbf{p}, \omega_i) \right)^2 \right) \quad (5)$$

where \mathbf{p} denotes a vector of p_j (with $j \in [1, \dots, N_p]$) properties to be obtained, m denotes the mode (with $m \in [1, \dots, M]$) and i is the index of the measured point (with $i \in [1, \dots, N_\omega]$) and N_ω the number of frequencies of the mode m).

The function $D(\mathbf{p})$ has N_p parameters and its global minimum is usually found by successive calculations with different values of \mathbf{p} . With this approach, the difference between the target wavenumber and the forward wavenumber is contained in a unique number $D(\mathbf{p})$. Consequently, the sensitivity of each wavenumber $k_{m,j}(\mathbf{p}, \omega)$ is not taken into account separately. The sensitivity of the wavenumbers can be encoded by defining a new function $F(\mathbf{p})$, a vector containing the $N_c =$

$\sum_{m=1}^M N_\omega^m$ scalar terms $F_{m,j}(\mathbf{p})$:

$$F(\mathbf{p}) = \begin{cases} F_{1,1}(\mathbf{p}) = k_{1,1}^{tar}(\omega_1) - k_{1,1}(\mathbf{p}, \omega_1) \\ \dots \\ F_{m,j}(\mathbf{p}) = k_{m,j}^{tar}(\omega_i) - k_{m,j}(\mathbf{p}, \omega_i) \\ \dots \\ F_{M,N_c}(\mathbf{p}) = k_{M,N_c}^{tar}(\omega_{N_c}) - k_{M,N_c}(\mathbf{p}, \omega_{N_c}) \end{cases}$$

From this formalism and because $N_c \gg N_p$, one can use a Gauss-Newton (GNA) algorithm to approximate the roots of $F(\mathbf{p})$ by an iterative process. The use of the regularized Gauss-Newton algorithm on an over-determined system of equations has shown good performance as well as quick convergence [11,19]. The estimation of the set of parameters \mathbf{p} at the iteration $n+1$ is given by Eq. (6).

$$\mathbf{p}^{n+1} = \mathbf{p}^n - J_F(\mathbf{p}^n)^{-1} F(\mathbf{p}^n) \quad (6)$$

with $J_F(\mathbf{p})$ ($N_c \times N_p$) the Jacobian matrix of the function $F(\mathbf{p})$ of expression :

$$J_F(\mathbf{p}) = \begin{bmatrix} \frac{\partial F_{1,1}(\mathbf{p})}{\partial p_1} & \dots & \frac{\partial F_{1,1}(\mathbf{p})}{\partial p_{N_p}} \\ \dots & \frac{\partial F_{m,j}(\mathbf{p})}{\partial p_j} & \dots \\ \frac{\partial F_{M,N_c}(\mathbf{p})}{\partial p_1} & \dots & \frac{\partial F_{M,N_c}(\mathbf{p})}{\partial p_{N_p}} \end{bmatrix}$$

Since the Jacobian matrix is rectangular, its Moore-Penrose pseudo-inverse can be expressed $(J_F(\mathbf{p}^n)^+ J_F(\mathbf{p}^n))^{-1} J_F(\mathbf{p}^n)^+$, where the superscript $+$ denotes transposition and complex conjugation [23,24]. With the expression of the pseudo-inverse of the Jacobian matrix, Eq. (6) becomes :

$$\mathbf{p}^{n+1} = \mathbf{p}^n - [(J_F(\mathbf{p}^n)^+ J_F(\mathbf{p}^n))^{-1} J_F(\mathbf{p}^n)^+] F(\mathbf{p}^n) \quad (7)$$

In addition, it can be shown that the terms inside the Jacobian matrix relate the sensitivity of a mode m to a parameter p_j . This means that if the material is isotropic, the Jacobian matrix can be calculated analytically, as shown in Eq. (8).

$$\frac{\partial F_{m,j}(\mathbf{p})}{\partial p_j} = - \frac{\partial k_{m,j}(\mathbf{p}, \omega_i)}{\partial p_j} = -S_{p_j}(\omega_i) \quad (8)$$

Table 3
Optimized parameters obtained by Gauss-Newton algorithm (GNA) and Genetic Algorithm (GA)

	Initial values	Gauss-Newton Algorithm (GNA)				Genetic Algorithm (GA)
		t = 1	t = 2	t = 4	Analytical	
$\overline{C_{11}} \pm \sigma_{C_{11}}$ (GPa)	$8.07+0.34i \pm 1.26+0.05i$	$8.49+0.36i \pm 0.03+0.01i$	$8.50+0.36i \pm (4.3+0.9i) \times 10^{-3}$	$8.49+0.36i \pm (5.32+1.27i) \times 10^{-3}$	$8.50+0.36i \pm (4.63+3.35i) \times 10^{-7}$	$8.44+0.36i \pm 0.19+0.01i$
$\overline{C_{66}} \pm \sigma_{C_{66}}$ (GPa)	$2.06+0.09i \pm 0.33+0.01i$	$2.50+0.1i \pm (1.09+4.18i) \times 10^{-4}$	$2.50+0.1i \pm (1.76+0.9i) \times 10^{-4}$	$2.50+0.1i \pm (2.96+1.67i) \times 10^{-4}$	$2.50+0.1i \pm (1.11+0.83i) \times 10^{-7}$	$2.49+0.1i \pm (2.88+0.13i) \times 10^{-2}$
$\overline{e} \pm \sigma_e$ (mm)	3.81 ± 0.29	$3.90 \pm 3.2 \times 10^{-3}$	$3.90 \pm 7.3 \times 10^{-5}$	$3.90 \pm 2.9 \times 10^{-4}$	$3.90 \pm 1.6 \times 10^{-7}$	3.89 ± 0.03
$\overline{D} \pm \sigma_D$ (rad/mm) ²	7.92 ± 7.73	$1.68 \times 10^{-4} \pm 4.08 \times 10^{-4}$	$0.78 \times 10^{-5} \pm 1.17 \times 10^{-5}$	$2.17 \times 10^{-5} \pm 2.64 \times 10^{-5}$	$0.76 \times 10^{-6} \pm 2.17 \times 10^{-6}$	$2.06 \times 10^{-2} \pm 6.48 \times 10^{-2}$
$\overline{N_{iter}} \pm \sigma_{N_{iter}}$		4 ± 1	4 ± 1	5 ± 1	4 ± 1	277 ± 101
$\overline{T} \pm \sigma_T$ (s)		81 ± 18	148 ± 24	223 ± 41	18 ± 3	7537 ± 2754

4. Case studies

4.1. Simulated experimental data for an isotropic viscoelastic plate

For validation purposes, the characterization of viscoelastic moduli and thickness is first tested using numerically simulated experimental data for an isotropic plate. The interest is that the sought parameters, i.e., viscoelastic moduli and plate thickness, are known (as used as input data), thus the efficiency and robustness of the method can be evaluated. Simulated dispersion curves are produced with the set of parameters \mathbf{p} obtained by a reference method and given in Section 2: $C_{11} = (8.5 + 0.36i)$ GPa, $C_{66} = (2.5 + 0.1i)$ GPa, $e = 3.90$ mm and $\rho = 1200$ kg m⁻³. The goal here is to evaluate the accuracy of the inversion procedure and to show that the algorithm is able to simultaneously assess the values of viscoelastic moduli and the thickness of a material plate.

Since inverse problems solved with the GNA are usually dependent on the initial guess, the algorithm is executed 20 times with random initial values δC_{ij} chosen within a range of $\pm 25\%$ around the exact viscoelastic moduli. Since high order modes are considered in the dataset, the value of their cut-off frequencies must be preserved at the first iteration, thus the initial perturbation for the thickness is set to $\sqrt{\delta C_{ij}}$. The converging criterion is set according to Eq. (6) by using a relative criterion of 0.05 % of the parameters. Optimization is performed for the 20 sets of initial parameters using the proposed approach with the analytical form of the sensitivity $S_{p_j}(\omega)$ and the approximated form $S_{p_j}^{(t)}(\omega)$ for different orders t of approximation, as presented in Section 2. Moreover, optimization is carried out using a genetic algorithm (GA) which involves evolutionary operator to find the global minimum of a multi-variable function. The following parameters are chosen for GA: number of individuals in the population = 4, maximum level of mutation = 5 %. The GA stops as soon as there is no change in the cost function over 50 generations meaning that the algorithm "reached" the global minimum. The cost function is defined as the sum of the squared distances between the dispersion curves shown as in Eq. (5) and is also calculated for the GNA to compare the performance of both algorithms.

The results are summarized in Table 3. The rows represents the mean values of the different parameters and the standard deviation over 20 optimizations. The first three rows represent the values of the optimized parameters and the last three represent the value of the cost function, the number of iterations needed for convergence and the optimization time respectively.

As shown in Table 3, the differences in the optimized properties between the proposed approach and the genetic algorithm are small. For the GNA, the relative difference between the optimized properties and the expected properties is less than 1%. The standard deviation on the optimized parameters reflects that this type of algorithm converges

toward the same value, even for different initial values. It should be pointed out that since the generated input data are noise free, the inverse problem is well conditioned. This contributes to making the standard deviation of parameters and the cost function very small. From a general point of view, the GNA is accurate for both exact and approximated formulations of the derivative. The change in order of approximation has an impact mainly on the number of iterations required for convergence and also on the time required for optimization. If the derivative cannot be estimated analytically, and depending on the accuracy required on the optimized properties, an order of approximation of $t = 2$ is the best order choice for solving this inverse problem since the precision is comparable to that obtained using $t = 4$, but with a lower computation time.

The use of the analytical form in the optimization procedure ensures very good accuracy in the optimized properties since the expression of the derivative is exact, while reducing the computation time significantly. Compared to the results obtained with the order of approximation $t=2$, the analytical form of the derivative provides standard deviations of the optimized parameters that are approximately 10.000, 1.000 and 100 times lower for C_{11} , C_{66} and e respectively.

In Table 3 it appears that the GA gives very good results too in terms of optimized properties, with less than 1% of relative error compared to the expected values. The standard deviation of optimized properties reflects that this type of algorithm does not always lead to the same optimized solution. This observation is reinforced by the very different cost function values obtained over 20 algorithms. In addition, it can be noticed that the mean value of the cost function obtained with the genetic algorithm is about twenty thousand times higher than that obtained with the GNA, using the analytical form of the derivative.

4.2. Measured experimental data for an isotropic viscoelastic plate

4.2.1. Experimental setup

Since it is difficult to measure the attenuation of many Lamb modes propagating simultaneously, as noted in [25], the experimental procedure is divided into two steps. The first one is an experimental measurement of the real part of the wavenumbers to estimate the coincidence angle of the propagating modes. To this end, a direct contact piezoelectric (PZT) transducer of diameter 45 mm with central frequency $f_0 = 250$ kHz (IMASONIC A101) coupled to the plate with gel is used as an emitter and the receiver is an air-coupled capacitive transducer of active area 3.3×10^3 mm² with a large angular aperture ($\approx [0;20]$ degrees) and large frequency bandwidth ($\approx [100;500]$ kHz down to -15 dB). As reported in [26], with this experimental setup it is possible to simultaneously generate and detect multiple Lamb wave modes propagating along a plate. The received signal is amplified with a Cooknell CA7/C charge amplifier. The configuration used for this

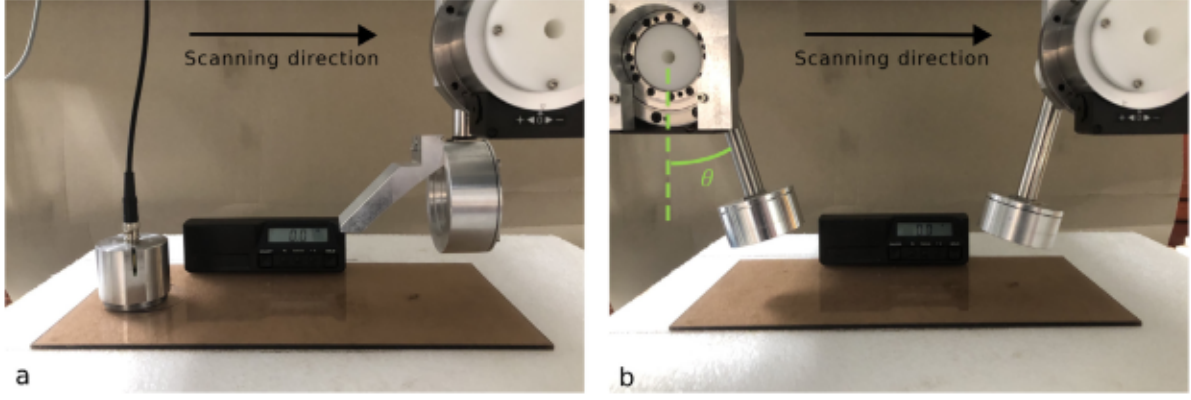


Fig. 2. (a) : Experimental setup with PZT emitter and air-coupled capacitive receiver. (b) Experimental setup with two air coupled capacitive ultrasonic transducers.

experiment is shown in Fig. 2(a). The input signal is a ten cycle sine burst centered at $f = 350$ kHz to excite multiple Lamb modes in the plate. To measure the wavenumbers of Lamb waves propagating in the plate, temporal signals are picked up for different positions of the receiver along the propagation path. The spatial step Δx is 1 mm and the total displacement of the receiver is 150 mm, thus the Shannon theorem is satisfied for all wavelengths and even the largest wavelength is well captured. The Perspex plate considered in the experimental part is rectangular of dimensions 390 mm \times 200 mm with a thickness of 3.90 ± 0.02 mm measured using a caliper.

To post-process signals measured in the space-time domain, a Fourier transform is applied to convert the time scale into frequency scale. The matrix pencil method is then applied to the resulting spacial-frequency matrix and chosen for its high robustness to noisy data [27]. Each experimental spectrum $u(x_n, \omega)$ measured at position $x = x_n$ ($n \in [1, N_x]$ where N_x is the number of spatial acquisition points) is then approximated by the following equation [28]:

$$u(x_n, \omega) \approx \sum_m^M a_m(x_1, \omega) e^{-i k_m(n-1)\Delta x} \quad (9)$$

Where M is the number of modes sought, $a_m(x_1, \omega)$ is the amplitude of the mode m measured at the first position along the path of displacement of the receiver, $k_m = k'_m + i k''_m$ the complex wavenumber of the mode m and Δx is the spatial acquisition step. Then, two new Hankel matrices X_1 and X_2 containing the acquired experimental signals are built :

$$X_1(\omega) = \begin{bmatrix} u(x_1, \omega) & \dots & u(x_L, \omega) \\ \vdots & \ddots & \vdots \\ u(x_{N_x-L}, \omega) & \dots & u(x_{N_x-1}, \omega) \end{bmatrix}$$

$$X_2(\omega) = \begin{bmatrix} u(x_2, \omega) & \dots & u(x_{L+1}, \omega) \\ \vdots & \ddots & \vdots \\ u(x_{N_x-L+1}, \omega) & \dots & u(x_{N_x}, \omega) \end{bmatrix}$$

Where L is the pencil parameter, intrinsic to the matrix pencil method and is generally chosen as $N_x/3 < L < N_x/2$ [29,30]. These matrices allow to express Eq. (9) as :

$$X_2 = X_1 e^{-i k_m \Delta x} \quad (10)$$

Next, a singular value decomposition is done on matrix X_1 such as $X_1 = U S V$ to find the M singular values that are attributed to the Lamb modes and the other singular values are associated to noise and are not conserved. Finally, Eq. (10) can be re-written:

$$Z = e^{-i k_m \Delta x} \quad (11)$$

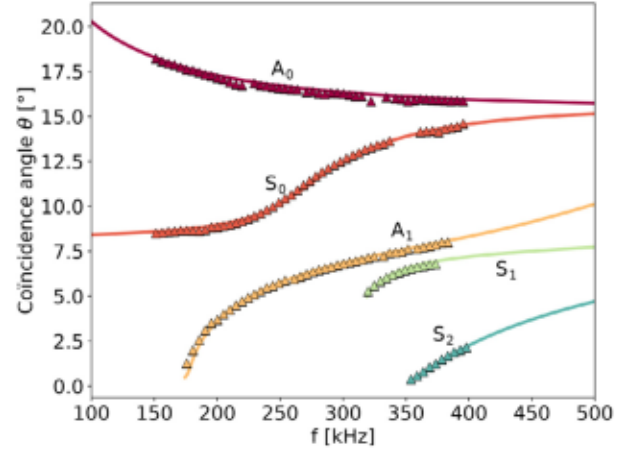


Fig. 3. Measured coincidence angle (triangle) and calculated coincidence angle with viscoelastic moduli and thickness given by reference method (solid line) as a function of frequency.

With $Z = S^{-1} U^T V^T X_2$ and the eigenvalues λ_m of Z allows to obtain the complex value of the wavenumber of mode m :

$$k'_m(\omega_m) = \frac{\Im[\ln(\lambda_m)]}{\Delta x} \quad (12)$$

$$k''_m(\omega_m) = \frac{\Re[\ln(\lambda_m)]}{\Delta x} \quad (13)$$

Additional details on the matrix pencil method can be found in [27,28].

The first experimental step shown in Fig. 2(a) and the above-described post-processing allow the real parts of the wavenumbers to be determined and in turn the coincidence angles of Lamb modes as a function of frequency. The coincidence principle occurs when the component of the incident (or radiated) wavenumber in the direction of propagation, k_x , is equal to the wavenumber of the Lamb mode m , k_m . This equality is also written:

$$\theta_m = \arcsin\left(\frac{k_m}{k_0}\right) \quad (14)$$

Where θ_m is the angle of the incident (or radiated) wave and k_0 is the wavenumber of the incident wave in air. From the previous equation, it is deduced that the coincidence angle θ_m is the angle at which the transducer should be inclined to generate (or detect) the mode m in the plate.

Next, the second experimental step is achieved consisting in using a pair of air-coupled capacitive transducers with narrow angular aperture, so that they are strongly mode selective. These are circular plane

Table 4

Optimization results obtained from reference method (two first column) and obtained from proposed guided waves method (last column).

	Reference through-transmission method in air [21]	Reference through-transmission method in water [21]	Proposed guided waves method
C_{11} (GPa)	$8.5 + 0.36i \pm 0.1 + 0.02i$	$8.9 + 0.2i \pm 0.6 + 0.1i$	$8.91 + 0.16i \pm 0.16 + 0.01i$
C_{66} (GPa)	$2.5 + 0.1i \pm 0.2 + 0.1i$	$2.3 + 0.06i \pm 0.02 + 0.03i$	$2.26 + 0.05i \pm 0.05 + 0.001i$
e (mm)	3.90 (fixed)	3.90 (fixed)	3.93 ± 0.02

elements of 52 mm in diameter, successively inclined at the above-mentioned angles, to generate-detect pure Lamb modes, as shown in Fig. 2(b). Angle control is provided by a numerically controlled goniometer with 0.01 degree precision. As in the first experimental step, the receiver is moved by 150 mm with spatial step of 1 mm to quantify the amplitude decay of each Lamb mode along its propagation path. The complex wavenumbers are then extracted using the matrix pencil method as explained in the first experimental step.

4.2.2. Experimental results

The coincidence angles extracted from the post-processing of the wavenumber measured with the experimental setup depicted in Fig. 2(a) are represented by the triangles in Fig. 3. The solid line represents the coincidence angle calculated using the viscoelastic moduli and thickness given by the reference method in Section 2 and shows a very good agreement with the measurements. The experimental setup presented in Fig. 2(b) is then used to measure the five modes separately in order to estimate the wavenumber k' and the attenuation k'' of each of them. The obtained dataset is then used to solve the inverse problem to optimize, at the same time, the viscoelastic moduli C_{11} , C_{66} and the thickness e of the material.

The initial guesses chosen for the set of parameters $\mathbf{p} = [C_{11}, C_{66}, e]$ are respectively $6.38 + 0.064i$ GPa, $1.88 + 0.02i$ GPa, 3.38 mm, corresponding to a difference of 25% with respect to the reference viscoelastic moduli and a difference of approximately 13% compared to the reference thickness. The initial dispersion curves calculated with this set of parameter $k(\mathbf{p})$ are represented by the dashed line in Fig. 4 as well as the experimental dataset k^{tar} that represents the target to be achieved. The algorithm converges after 6 iterations in about 12s, which enables us to find the optimized set of parameters \mathbf{p}^{opt} . The dispersion curves calculated with the optimized set of parameters $k(\mathbf{p}^{opt})$ represent wavenumbers that best fit the experimental wavenumbers k^{tar} and are represented by solid line in Fig. 4.

Experimental errors are taken into account by considering a non-perfect parallelism between the line along which the receiver is moved and the plate surface [31]. For a mode m , the ratio of the apparent wavenumber measured with a mismatch angle ϕ to the "true" wavenumber k_m can be defined as :

$$\Delta k_m = \cos \phi + \frac{\sin |\phi|}{\tan \theta_m}$$

The uncertainties are then computed in cases where $\phi \pm 0.1$ degrees, thus making it possible to create two new sets of dispersion curves, $k^{tar} \pm \Delta k_m$ representing data that could have been measured if an error had been made in the parallelism. These errors are represented for each mode by the shadow zones in Fig. 4 and the effect of these errors on the optimized material properties is calculated using a Newton algorithm as shown in [32]. The optimized parameters with uncertainties are presented in Table 4. Cross experiments have been performed to verify the accuracy of the proposed method, using a robust ultrasonic immersion technique [21]. The viscoelastic moduli thus obtained for the Perspex plate sample are also provided in Table 4 for validation purpose.

The optimized values of the real part of the viscoelastic moduli are very close to those obtained with the reference method applied when the plate sample is either in air or in water. The relative difference in C'_{11} is less than 5% compared to that obtained by the reference method, while the relative difference in C'_{66} is about 10% compared to the reference method in air and less than 2% compared to the reference in water. The imaginary parts of the viscoelastic moduli are estimated with a larger relative differences. Compared to the reference method in water, the relative differences are about 20% and 17% for C''_{11} and C''_{66} respectively. Finally, the thickness optimized from the guided waves dataset is very close to that measured using a caliper (3.90 ± 0.02 mm), which represents a relative error of less than 1%. Specific measurements using non-viscoelastic plates (or with negligible level of viscosity), e.g. made of metal or glass, have shown that the loss in amplitude due to the angular opening of the guided ultrasonic beams can be neglected when compared to the loss due to viscoelastic effects in the Perspex plate. In this way, the imaginary parts of the evaluated C_{11} and C_{66} are assumed to be representative of the viscoelasticity of the Perspex.

5. Conclusion

In this paper, the sensitivity of Lamb waves to the viscoelastic properties and thickness of isotropic plates has been derived and used to formulate an inverse problem. For numerically computed dispersion curves, it has been shown that the using of the Gauss-Newton algorithm provides the solution much more quickly and with a better accuracy than a genetic algorithm. In addition, the explicit formulation of the derivative of the wavenumber with respect to a given material parameter makes the process even faster because there is no need to numerically estimate the derivative of the wavenumber using a conventional approximated method. The algorithm was successfully tested for experimental data and showed high robustness when measured complex wavenumbers were used to assess complex elastic moduli of a polymer-like material plate. The experimental process consisted in two steps: one was multimodal generation and detection to quickly estimate the coincidence angles of all Lamb modes in a frequency range of a few hundred kHz, using one contact PZT transmitter coupled with gel and one air-coupled capacitive receiver; the second step consisted in a mode selective process (based on the use of the previously measured angles) to accurately evaluate the wavenumber and attenuation of each mode. The first step could potentially be removed if the material properties were known approximately (for instance to monitor material aging). In this way, the material characterization would be totally contact-less in addition to being single-sided access, thus offering great convenience for in-situ NDE applications, e.g., to monitor the thickness and viscoelastic moduli of mounted components made of various materials, by simply bringing in the pair of air-coupled transducers and placing them properly one side of the tested panel. The optimized properties show very good agreement with reference values obtained using a well established through-transmission method, with the plate sample being placed in air or into water. Finally, using the proposed method, it is possible in just a few second to simultaneously estimate the viscoelastic

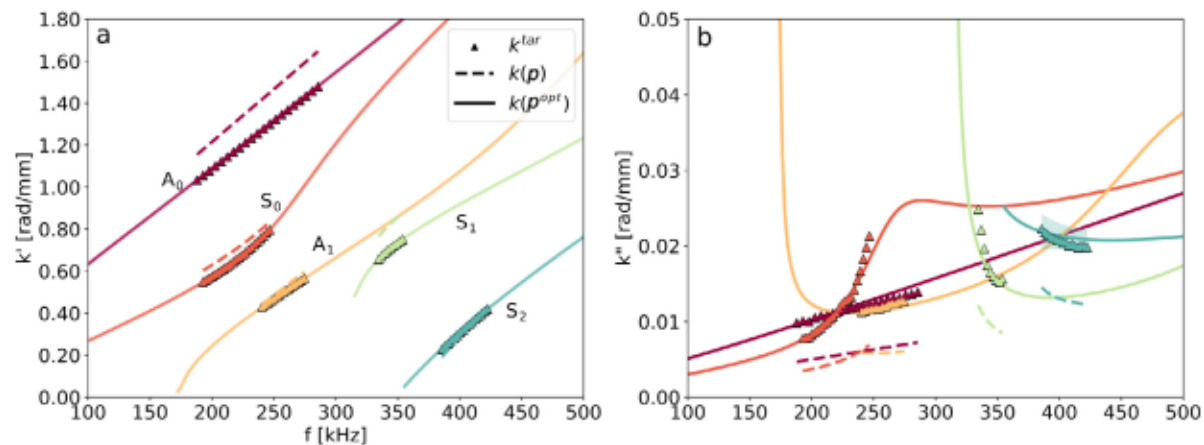


Fig. 4. (a) : Real part of the wavenumber as a function of frequency. (b) Imaginary part of the wavenumber as a function of frequency. Initial dispersion curves (dashed line), measured dispersion curves (triangles) and optimized dispersion curves (solid line).

moduli and the thickness of the plate using single-sided experimental setup in air. To go further, the analytical form of the derivative could be calculated for more complex structures such as adhesively bonded assemblies. This work is in progress and should make it possible to quickly assess the viscoelastic moduli and the thickness of the adhesive layer, which is of great interest in an industrial context.

CRedit authorship contribution statement

Clément Despres: Writing – original draft, Visualization, Validation, Software, Resources, Project administration, Methodology, Investigation, Data curation, Conceptualization. **Christine Biateau:** Resources, Data curation. **Michel Castaings:** Validation, Supervision, Resources, Project administration, Methodology, Formal analysis. **Nicolas Quaegebeur:** Validation, Project administration, Methodology, Funding acquisition, Formal analysis, Conceptualization. **Patrice Masson:** Validation, Supervision, Project administration, Methodology, Funding acquisition, Conceptualization. **Eric Ducasse:** Validation, Project administration, Methodology, Formal analysis, Conceptualization.

Declaration of competing interest

The authors declare that they have no known competing financial interests or personal relationships that could have appeared to influence the work reported in this paper.

Data availability

The authors are unable or have chosen not to specify which data has been used.

Acknowledgments

The authors would like to acknowledge the support of the Natural Sciences and Engineering Research Council of Canada (NSERC) and the “Fonds de Recherche du Québec - Nature et Technologies” (FRQNT) for their fundings.

References

- [1] Nguyen K-CT, Le L, Tran T, Sacchi M, Lou E. Excitation of ultrasonic lamb waves using a phased array system with two array probes: Phantom and in vitro bone studies. *Ultrasonics* 2013;54. <http://dx.doi.org/10.1016/j.ultras.2013.08.004>.
- [2] Hosten B, Castaings M. Validation at lower frequencies of the effective elastic constants measurements for orthotropic composite materials. In: *Review of progress in quantitative nondestructive evaluation*. 1993. http://dx.doi.org/10.1007/978-1-4615-2848-7_153.
- [3] Fei D, Chimenti DE. Single-scan elastic property estimation in plates. *Acoust Res Lett Onl* 2001;2(1):49–54. <http://dx.doi.org/10.1121/1.1353376>.
- [4] Orta A, Segers J, Vandendriessche J, Roozen N, Van Paepegem W, Kersemans M, et al. Characterization of the orthotropic elastic tensor of composites using full-field Lamb waves. 2020. <http://dx.doi.org/10.48465/fa.2020.0909>.
- [5] Castaings M, Cawley P. The generation, propagation, and detection of Lamb waves in plates using air-coupled ultrasonic transducers. *J Acoust Soc Am* 1996;100(5):3070–7. <http://dx.doi.org/10.1121/1.417193>.
- [6] Bochud N, Jérôme L, Bruno F, Royer D, Prada C. Towards real-time assessment of anisotropic plate properties using elastic guided waves. *J Acoust Soc Am* 2018;143. <http://dx.doi.org/10.1121/1.5024353>.
- [7] Hosten B, Castaings M, Tretout H, Voillaume H. Identification of composite materials elastic moduli from lamb wave velocities measured with single sided, contactless ultrasonic method. *AIP Conf Proc* 2001;557:1023–30. <http://dx.doi.org/10.1063/1.1373867>.
- [8] Ostiguy P-C, Quaegebeur N, Masson P. Non-destructive evaluation of coating thickness using guided waves. *NDT E Int* 2015;76:17–25. <http://dx.doi.org/10.1016/j.ndteint.2015.08.004>.
- [9] Moilanen P, Nicholson PHF, Kilappa V, Cheng S, Timonen J. Assessment of the cortical bone thickness using ultrasonic guided waves: Modelling and in vitro study. *Ultrasound Med Biol* 2007;33(2):254–62. <http://dx.doi.org/10.1016/j.ultrasmedbio.2006.07.038>.
- [10] Karim MR, Mal AK, Bar-Cohen Y. Inversion of leaky Lamb wave data by simplex algorithm. *J Acoust Soc Am* 1990;88(1):482–91. <http://dx.doi.org/10.1121/1.399927>.
- [11] Rupitsch S, Ilg J. Complete characterization of piezoceramic materials by means of two block-shaped test samples. *IEEE Trans Ultrason Ferroelectr Freq Control* 2015;62:1403–13. <http://dx.doi.org/10.1109/TUFFC.2015.006997>.
- [12] Bauer F, Hohage T, Munk A. Iteratively regularized Gauss-Newton method for nonlinear inverse problems with random noise. *SIAM J Numer Anal* 2009;47:1827–46. <http://dx.doi.org/10.1137/080721789>.
- [13] Bochud N, Vallet Q, Bala Y, Follet H, Minonzio JG, Laugier P. Genetic algorithms-based inversion of multimode guided waves for cortical bone characterization. *Phys Med Biol* 2016;61:19:6953–74. <http://dx.doi.org/10.1088/0031-9155/61/19/6953>.
- [14] Eremin A, Glushkov E, Glushkova N, Lammering R. Evaluation of effective elastic properties of layered composite fiber-reinforced plastic plates by piezoelectrically induced guided waves and laser Doppler vibrometry. *Compos Struct* 2015;125. <http://dx.doi.org/10.1016/j.compstruct.2015.02.029>.
- [15] Bonyadi MR, Michalewicz Z. Particle swarm optimization for single objective continuous space problems: A review. *Evol Comput* 2017;25:1–54. http://dx.doi.org/10.1162/EVCO_r_00180.
- [16] Qi C, Xu K, Ta D. High-resolution Lamb waves dispersion curves estimation and elastic property inversion. *Ultrasonics* 2021;115. <http://dx.doi.org/10.1016/j.ultras.2021.106427>.
- [17] Gopalakrishnan K, Rautela M, Deng Y. Deep learning based identification of elastic properties using ultrasonic guided waves. In: Rizzo P, Milazzo A, editors. *European workshop on structural health monitoring. EWSHM 2020. lect. notes civ. eng.*, vol. 128. Cham: Springer International Publishing; 2021. p. 77–90. http://dx.doi.org/10.1007/978-3-030-64908-1_8.
- [18] Kudela P, Radzienski M, Fiborek P, Wandowski T. Elastic constants identification of woven fabric reinforced composites by using guided wave dispersion curves and genetic algorithm. *Compos Struct* 2020;249:112569. <http://dx.doi.org/10.1016/j.compstruct.2020.112569>.

- [19] Ponschab M, Kiefer D, Rupitsch S. Simulation-based characterization of mechanical parameters and thickness of homogeneous plates using guided waves. *IEEE Trans Ultrason Ferroelectr Freq Control* 2019;PP:1. <http://dx.doi.org/10.1109/TUFFC.2019.2933699>.
- [20] Royer D, Dieulesaint E. *Elastic waves in solids I. Free and guided propagation*. Berlin, Heidelberg: Springer; 1999.
- [21] Castaings M, Hosten B. Air-coupled measurement of plane wave, ultrasonic plate transmission for characterising anisotropic, viscoelastic materials. *Ultrasonics* 2000;38(1):781–6. [http://dx.doi.org/10.1016/S0041-624X\(99\)00036-0](http://dx.doi.org/10.1016/S0041-624X(99)00036-0).
- [22] Rose Joseph L. *Ultrasonic guided waves in solid media*. Cambridge University Press; 2014.
- [23] Moore EH. On the reciprocal of the general algebraic matrix (abstract). *Bull Am Math* 1920;26:394–5.
- [24] Penrose R. A generalized inverse for matrices. *Math Proc Cambridge Philos* 1955;51:406–13. <http://dx.doi.org/10.1017/S0305004100030401>.
- [25] Kerber F, Sprenger H, Niethammer M, Luangvilai K, Jacobs L. Attenuation analysis of lamb waves using the chirplet transform. *EURASIP J Adv Signal Process* 2010. <http://dx.doi.org/10.1155/2010/375171>.
- [26] Hosten B, Castaings M. Parabolic mirror and air-coupled transducer for multi-modal plate wave detection. *AIP Conf Proc* 2003;657(1):1243–50. <http://dx.doi.org/10.1063/1.1570274>.
- [27] Chang CY, Yuan FG. Extraction of guided wave dispersion curve in isotropic and anisotropic materials by Matrix Pencil method. 89, 2018, p. 143–54. <http://dx.doi.org/10.1016/j.ultras.2018.05.003>.
- [28] Cao X, Zeng L, Lin J. Lamb wave mode decomposition and reconstruction based on the viscoelastic propagation model. *Struct Health Monit* 2020;20:147592172091499. <http://dx.doi.org/10.1177/1475921720914992>.
- [29] Schöpfer F, Binder F, Wöstehoff A, Schuster Thomas, Ende Sven, Föll S, et al. Accurate determination of dispersion curves of guided waves in plates by applying the matrix pencil method to laser vibrometer measurement data. *CEAS Aeronaut J* 2013;4. <http://dx.doi.org/10.1007/s13272-012-0055-7>.
- [30] Sarkar TK, Pereira O. Using the matrix pencil method to estimate the parameters of a sum of complex exponentials. *IEEE Antennas Propag Mag* 1995;37(1):48–55. <http://dx.doi.org/10.1109/74.370583>.
- [31] Moreau L, Minonzio JG, Foirer J, Bossy E, Talmant M, Laugier P. Accurate measurement of guided modes in a plate using a bidirectional approach. *J Acoust Soc Am* 2014;135:EL15–21. <http://dx.doi.org/10.1121/1.4832335>.
- [32] Baudouin S, Hosten B. Comparison between prediction and measurement of viscoelastic moduli in composite materials versus temperature using ultrasonic immersion technique with oil. *J Acoust Soc Am* 1997;102(6):3450–7. <http://dx.doi.org/10.1121/1.419587>.